Modeling the radiative properties of dense plasmas

P. Gauthier and S. J. Rose
Plasma Physics Group, Rutherford Appleton Laboratory, Chilton, Didcot OX11 0QX, United Kingdom

P. Sauvan, P. Angelo, and E. Leboucher-Dalimier
Physique Atomique dans les Plasmas Denses, LULI, CNRS, Université Paris VI, 4 Place Jussieu, 75252 Paris Cedex 05, France and Ecole Polytechnique, 91128 Palaiseau, France

A. Calisti and B. Talin
Physique des Interactions Ioniques et Moléculaires, Université de Provence, Centre de St. Jérome, 13397 Marseille, France
(Received 9 May 1997; revised manuscript received 2 February 1998)

A model aimed at describing the electronic structure of hot dense plasmas is presented. This model is first used to study the effect of the nearest neighbor interaction on the photoabsorption K-edge position in a dense fluorine plasma. Changes to the ionization potential lowering from the well-known ion sphere model [H. Nguyen *et al.*, Phys. Rev. A **33**, 1279 (1986)] are obtained by the present approach for plasma density above solid. We believe that this effect could be of importance in the calculation of the opacity of dense materials. The present model also provides an alternative to the treatment of line broadening in very dense plasmas where the average interionic spacing can be of the order of the spatial extent of the excited-state orbitals. To illustrate this point, we present F Lyman-β line shapes for various density conditions. [S1063-651X(98)01707-3]

PACS number(s): 52.25.Nr, 32.60+i, 32.30.Rj, 52.50.Jm

I. INTRODUCTION

There are many phenomena in astrophysics and inertial confinement fusion (ICF) that require an understanding of the effect of high material densities on the physical processes in a plasma. For example, the radiative properties of hot dense plasmas are of interest in studies of stellar structure and evolution [1,2]. The design of ICF targets to achieve a breaking even and gain also requires an accurate knowledge and understanding of the properties of such plasmas. Models of plasma behavior that work well for low densities are more questionable under these extreme conditions. We present in this paper a model for describing the radiative properties of hot dense plasmas. We consider particularly the regime in which modifications of the interatomic potentials of the ions by other ions substantially modify effects on radiative properties.

The electronic structure of a plasma ion depends on its interactions with the other plasma particles (ions and electrons). In standard line shape theories [3,4], the electronic structure is calculated by modeling the plasma by a set of independent cells, each containing a radiator and N perturbers (N ions$+N'$ free electrons). The perturbers, considered as point charged particles, are treated in classical mechanics, whereas the radiator is described in the frame of the quantum theory. The influence of the N ions on the electron orbitals of the radiator is then taken into account through an external field (Stark effect).

This representation is acceptable in the case of relatively dilute plasmas, where the mean interionic spacing R_i is much greater than the typical spatial extent r_n of the excited-state orbitals. In very dense plasmas, where R_i may be of the order of r_n, this description is more questionable. Indeed one has in this case to take specifically into account the possible overlapping of the most outer bound electron orbitals from neighboring ions. In this context, we believe that a better representation of the electronic structure is provided by the use of an $(N+1)$-center molecular basis. We also point out that such a description presents the strong advantage of leading to an exact treatment of the multipolar interaction to all orders.

In our model we assume that the influence of the plasma ions on the individual atomic bound states is well represented by the nearest neighbor (NN) interaction. We thus carried out the electronic structure calculations setting $N+1$ equal to 2. The validity of this assumption is discussed in this paper. Preliminary investigations of the electronic structure of dense plasmas in terms of two-center wave functions were reported by Malnoult *et al.* [5]. In this study, the uniform electron gas model was employed to assess the effect of the electronic component of the plasma on bound states, which is a description strictly valid for infinite electron temperatures. In our work, in order to take into account finite temperature effects, a self-consistent description for bound and free charges is used.

We calculate in Sec. II the electronic structure of a *two*-center system (also hereafter called a ''quasimolecule'') embedded in a dense plasma, consisting of a central ion of interest and its NN. To account for the distribution of internuclear separations in a real plasma, configurational averaging of the *two*-center calculations is performed using molecular dynamics (MD) simulations. In Sec. III we use these exploratory calculations to draw some general conclusions about the effect of the NN on the absorption K-edge position in dense fluorine plasmas. We more particularly investigate the change in the continuum-lowering energy resulting from our accurate treatment of the NN interaction. Finally we present in Sec. IV a series of line shape calculations based on our modeling.

Before going further in the presentation of our model, we

would like to emphasize that, due to the large ionic velocities involved, we do not consider in this work the possibility for molecular states to be established (as in a molecule bound by a chemical bond).

II. SELF-CONSISTENT-FIELD DESCRIPTION FOR A "QUASIMOLECULE" EMBEDDED IN A DENSE PLASMA

A. Description of the model

The model starts with the solution of the electronic part of the molecular Schrödinger equation in the Thomas-Fermi average potential and the calculation of the average one-electron properties (orbital energies, oscillator strengths). A cylindrically symmetric confining volume $\mathcal{V}$ is defined from the particular ionic equipotential that satisfies the electrical neutrality condition. Details about the calculation of $\mathcal{V}$ can be found in the work from Malnoult *et al.* [5]. In the present work, in order to include finite temperature effects, a self-consistent description for bound and free charges is used. More specifically, the total electrostatic potential generated in the confining cell by electrons and ions is obtained from the nonlinear Poisson equation:

$$\Delta V_{\rm tot}(\lambda,\mu,\varphi;R)=4\pi\left[n_f[V_{\rm tot}(\lambda,\mu,\varphi;R)]+n_b-\sum_{i=1,2}Z_i\delta(\vec{r}-\vec{r}_i)\right] \tag{1a}$$

with the Dirichlet boundary condition:

$$V_{\rm tot}(\text{confining surface})=0. \tag{1b}$$

In Eq. (1a) n_f and n_b are respectively the free and bound electron charge densities. The elliptical coordinates (λ,μ,φ) are used. They are related to the distance r_i of the bound electron from either of the nuclei of charge Z_i by

$$\lambda=\frac{r_1+r_2}{R},\quad \lambda=[1,+\infty],$$

$$\mu=\frac{r_1-r_2}{R},\quad \mu=[-1,+1], \tag{2}$$

$$\varphi\in[0,2\pi].$$

The distance R is the internuclear separation. In elliptical coordinates, the element of volume is

$$d\tau=\frac{R^3}{8}(\lambda^2-\mu^2)d\lambda\ d\mu\ d\varphi \tag{3}$$

and the Laplacian is given by

$$\Delta=\frac{4}{R^2(\lambda^2-\mu^2)}\left[\frac{\partial}{\partial\lambda}(\lambda^2-1)\frac{\partial}{\partial\lambda}+\frac{\partial}{\partial\mu}(1-\mu^2)\frac{\partial}{\partial\mu}+\frac{(\lambda^2-\mu^2)}{(\lambda^2-1)(1-\mu^2)}\frac{\partial^2}{\partial\varphi^2}\right]. \tag{4}$$

Because the system is invariant under rotation around the internuclear axis, the potential is in practice independent of the azimuthal angle φ. For electron temperature much greater than the plasma Fermi temperature, the Thomas-Fermi free-electron distribution can be expressed in terms of the total electrostatic potential $V_{\rm tot}$ by [6]

$$n_f(\lambda,\mu,\varphi;R)=\frac{N_eB(\lambda,\mu,\varphi;R)}{\frac{1}{\mathcal{V}}\int B(\lambda,\mu,\varphi;R)d\tau},$$

$$B(\lambda,\mu,\varphi;R)=\frac{2}{\sqrt{\pi}}u_0+e^{u_0^2}\,\mathrm{erfc}(u_0), \tag{5}$$

$$u_0=\left(\frac{V_{\rm tot}}{kT_e}\right)^{1/2},$$

where $\mathrm{erfc}(x)$ is the complementary error function [7]. N_e and T_e are, respectively, the mean electron density and the electron temperature. The bound electron eigenvalues and wave functions are obtained by solving the Schrödinger equation

$$[H_0-V(\lambda,\mu,\varphi;R)]\phi_{nlm}(\lambda,\mu,\varphi;R)=E_{nlm}(R)\phi_{nlm}(\lambda,\mu,\varphi;R),$$

$$H_0=-\frac{\Delta}{2}+\frac{Z_1Z_2}{R}+\frac{2\lambda(Z_1+Z_2)+2\mu(Z_1-Z_2)}{R(\lambda^2-\mu^2)}, \tag{6}$$

$$V=V_{\rm tot}-V_b.$$

In Eq. (6), $E_{nlm}(R)$ is the bound electron energy in the Born-Oppenheimer approximation and ϕ_{nlm} is the electron wave function with the corresponding spherical quantum numbers defined in the limit $R=0$. V_b is the bound electron potential energy. The Hamiltonian H_0 corresponds to the pure one-electron diatomic molecule free from plasma effects. Equations (1) and (6) are solved self-consistently for bound and free charges. At each iteration and for a given internuclear separation, the Poisson equation is solved according to a finite difference scheme at the nodes of a two-dimensional variable step elliptical mesh covering the whole confining volume. The eigenfunctions ϕ_{nlm} are taken as a linear combination of a set of 40 eigenfunctions $\phi^{(0)}_{nlm}$ of H_0 corresponding to the 40 lowest eigenvalues $E^{(0)}_{nlm}(R)$ of the pure one-electron diatomic molecule, namely,

$$\phi_{\alpha=\{nlm\}}=\sum_{\alpha'=\{n'l'm'\}}a_{\alpha\alpha'}(R)\phi^{(0)}_{\alpha'}. \tag{7}$$

The eigenfunctions $\phi^{(0)}_{nlm}$ and eigenvalues $E^{(0)}_{nlm}(R)$ are computed using a molecular physics code [8] in which the Schrödinger equation $H_0\ \phi^{(0)}_{nlm}=E^{(0)}_{nlm}(R)\ \phi^{(0)}_{nlm}$ is split in two (so-called "inner" and "outer") coupled equations [9,10]. A variational method is thus applied to compute the bound energy levels $E_{nlm}(R)$.

TABLE I. Variation of the electron density $n_e^{(0)}$ on the boundary of the confining cell as a function of the electron temperature. The computations were performed for a F^{8+} and a F^{9+} ion separated by $R=4$ a.u. For these calculations the mean electron density was $N_e=2\times10^{23}$ cm^{-3}.

T_e (eV)	$n_e^{(0)}/N_e$
100	0.88
200	0.93
300	0.95
500	0.96
700	0.97
1000	0.98
1500	0.998
3000	1.00
∞	1.00

B. First results

We show in Table I the variation of the electron density $n_e^{(0)}$ on the confining surface as a function of the electron temperature. Calculations were performed for a F^{8+} and a F^{9+} ion separated by $R=4$ a.u. The mean electron density was $N_e=2\times10^{23}$ cm^{-3}. As the temperature increases the calculation tends to the uniform electron gas limit $(n_e^{(0)}/N_e=1)$.

We also present in Fig. 1 views of the equipotential surfaces of the total self-consistent electrostatic potential $V_{\rm tot}$ generated by bound and free charges in the confining cell. Calculations concern again a (F^{8+}, F^{9+}) structure embedded in a dense ($N_e=2\times10^{23}$ cm^{-3}) hot ($T_e=300$ eV) plasma. Two internuclear separations are considered: $R=8$ a.u. (upper graph) and $R=4$ a.u. (lower graph). For the largest distance R considered here, it can be seen that electron screening effects overwhelm the NN interaction. Indeed the equipotential surfaces present an almost spherical symmetry and the internuclear region is dominated by negative values of the total potential. For $R=4$ a.u., the region of potential negative values disappears and the equipotential surfaces acquire a cylindrical symmetry. In these conditions the distortion of the ion wave functions is too great to be dealt with standard spherically symmetric models.

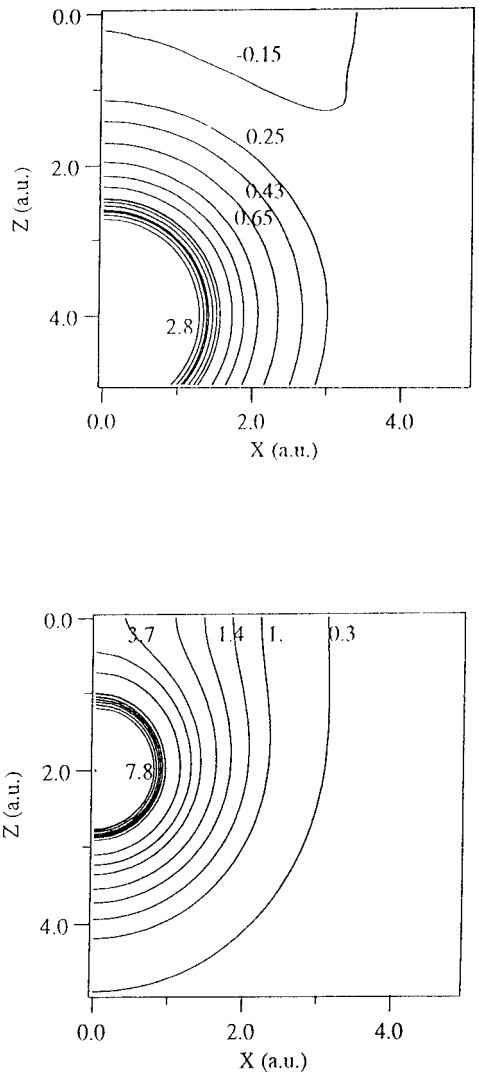

FIG. 1. Meridian lines of the equipotential surfaces relative to the total potential $V_{\rm tot}$ in the confining cell for two different internuclear distances: $R=8$ a.u. (upper graph) and $R=4$ a.u. (lower graph). Values of the potential indicated on the figure are expressed in atomic units. A quarter of the confining cell is represented. The nuclei are located at $(X=0, Z=\pm R/2)$. The equipotential lines correspond to a (F^{8+}, F^{9+}) two-center system in a dense ($N_e=2\times10^{23}$ cm^{-3}) hot ($T_e=300$ eV) plasma.

III. IONIZATION POTENTIAL LOWERING IN HOT DENSE PLASMAS

A. General considerations

In a plasma of finite density the potential distribution in and near a given ion is influenced not only by its own bound electrons but also by free electrons and by neighboring ions. The time-averaged effect of these perturbers is to alter the set of energy levels available to the ion in question. This effectively lowers all the ionization potentials and shifts the equilibrium occupation numbers in the direction of increased ionization. This effect (so-called ''pressure ionization'') has often been treated in a simplified way in the past within the ion sphere model, by assigning to each ion a sphere occupying the ion's share of the total volume and containing the ion and enough free electrons to make the sphere's net charge zero. In this approach, inside the sphere the potential due to the contents of neighboring spheres is neglected. Thus, close encounters between ions are disregarded, and the picture is basically that of a crystal lattice. In other words, the only time-averaged effect of plasma free electrons is considered in each confining cell. The quasimolecular approach gives rise to significant improvements to the ISM because the averaged effect of the NN, as well as the effect of free electrons, is taken into account in the calculation of the continuum-lowering energy. However, as internuclear distances greater than the plasma screening distance are probed, the two models come together. To illustrate this point, we compared the variation of the ground state energy of Ne^{9+} as a function of the electron temperature as calculated from the present approach with the one obtained in the ISM model by Nguyen

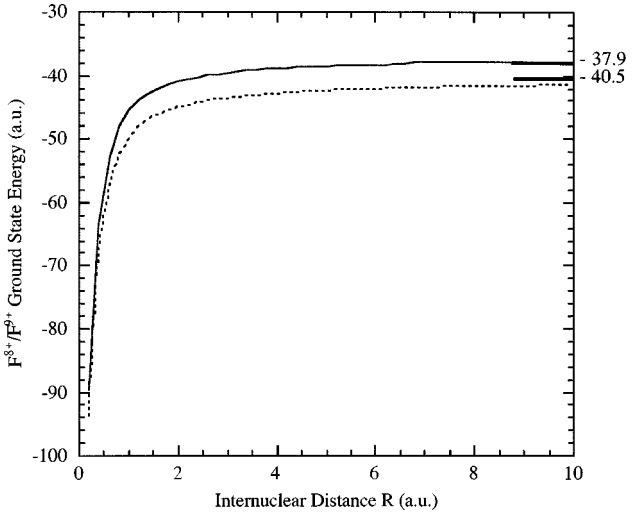

FIG. 2. Variation of the ground-state energy of a H-like fluorine ion as a function of its distance from its NN in the plasma for $N_e = 10^{23}$ cm^{-3}, $T_e = 300$ eV (solid line), and $N_e = 0$ (dotted line). The value -40.5 a.u. is the F^{8+} ground-state energy (i.e., $-Z^2/2$). In the case of the finite electron density plasma, the F^{8+} ground-state energy predicted by the ion sphere model (ISM) is progressively recovered as R increases. Significant corrections to the ISM energy appear for $R < 4$ a.u.

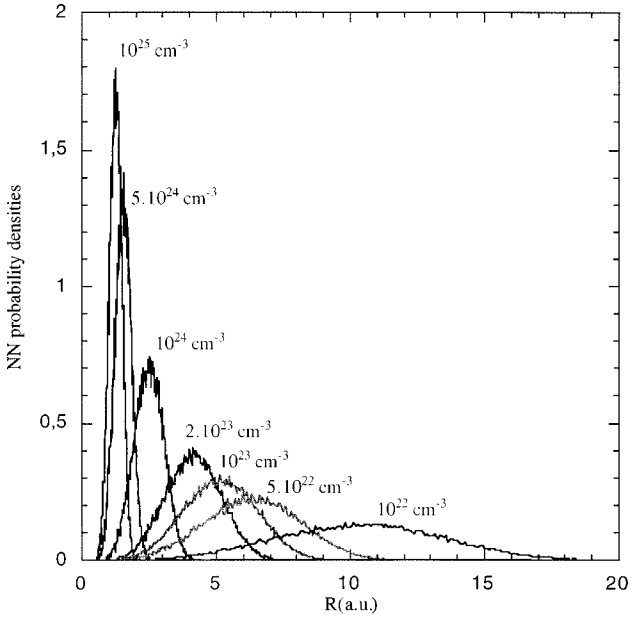

FIG. 3. Nearest neighbor probability densities in a fluorine plasma as computed from molecular dynamics simulations for different electron densities ranging from 10^{22} to 10^{25} cm^{-3}. The calculations were performed for the same electron temperature ($T_e = 300$ eV). The distributions are normalized to unity.

et al. [11]. The computations were performed for an electron density $N_e = 10^{24}$ cm^{-3}. The agreement is good: the relative discrepancy between the two models is always less than 0.3%.

B. Photoabsorption *K*-edge position in a dense fluorine plasma

Figure 2 shows the variation of the ground-state energy of a H-like fluorine ion as a function of the distance between an ion and its NN in the plasma. The solid curve corresponds to the case of a fluorine ion embedded in a high density ($N_e = 10^{23}$ cm^{-3}) high temperature ($T_e = 300$ eV) fluorine plasma and the dashed curve corresponds to the ground state of the same two-center structure but free from electron screening effects. The ground level $E_K(R; 10^{23}$ cm^{-3}, 300 eV) is less tightly bound in the presence of plasma free electrons as expected. For the solid curve, at large internuclear separations R the local field of the NN is totally shielded by the plasma free electrons and the ground-state energy becomes independent of R and identical to its ISM value. At smaller internuclear distances (i.e., < 4 a.u.) we observe an important variation of the ground-state energy as the electron screening is not sufficient to shield the NN interaction. We note that the lowering of the ionization potential is always larger in the ISM model.

A complete calculation of the edge position for a real plasma requires configurational averaging of the two-center calculations. To do this, we computed from molecular dynamics simulations [12–14] the probability $P_{\mathrm{NN}}(R)$ that a central ion of interest is separated by the distance R from its NN in a fluorine plasma. An effective screened potential was used for the ion-ion interaction, the interaction energy between two particles, i and j, being given by

$$\varphi(\vec{r}) = \frac{Z_i Z_j e^2}{|\vec{r}|} \exp\left(-\frac{|\vec{r}|}{L_s}\right), \qquad |\vec{r}| = |\vec{r}_i - \vec{r}_j|. \tag{8}$$

In practice, different screening distances L_s have been tested in our computations and the NN distributions were shown not to depend significantly on this parameter. Results presented in the following were obtained for a screening distance equal to the ion sphere radius R_0 defined by $(4\pi R_0^3/3)N_e + k = Z$.

In Fig. 3 we present NN probability densities for a large range of electron densities N_e from 10^{22} to 10^{25} cm^{-3} and for the same electron temperature $T_e = 300$ eV. As the density increases, the distributions are strongly narrowed and displaced towards the origin.

For given values of the electron density and temperature, the averaged over NN distances ground-state energy $I(N_e, T_e)$ is given by

$$I(N_e, T_e) = \frac{\int_0^\infty dR\ P_{\mathrm{NN}}(R; N_e, T_e) E_K(R; N_e, T_e)}{\int_0^\infty dR\ P_{\mathrm{NN}}(R; N_e, T_e)}. \tag{9}$$

Figure 4 shows the variation of this averaged ground-state energy for H-like fluorine as a function of the electron density. Results from the QM model are compared to the ones obtained in the ISM, also deduced from our two-center calculations in the limit of large internuclear separations. It is seen that the QM model and the ISM come together at densities lower than 10^{23} cm^{-3}. The difference between the two models increases as the electron density increases, i.e., when

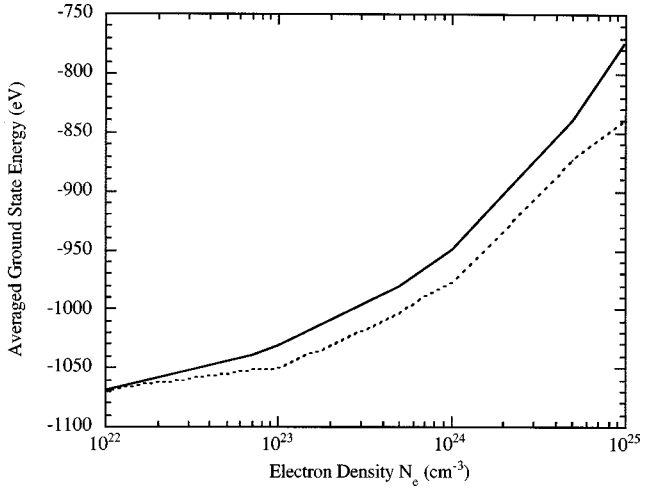

FIG. 4. Average ground-state energy of H-like fluorine as a function of the plasma electron density. Quasimolecular (QM) computations (dotted line) are compared with results from the ion sphere model (solid line). Calculations have been performed with $T_e=300$ eV. The discrepancy between the two models becomes obvious for $N_e>10^{23}$ cm^{-3}.

averaging is performed over internuclear separations smaller than the ion-sphere radius. In this case the neighboring fluorine ion acts to increase the nuclear charge that the inner shell bound electron ''sees'' and this is a larger effect than the introduction of the extra electronic charge inside ion volume. For an electron density $N_e=10^{25}$ cm^{-3}, the ionization potential lowering as calculated from the present approach is 70 eV smaller than the one deduced from the ISM calculations.

IV. LINE SHAPES IN VERY DENSE PLASMAS

A. Theoretical approach

Equipped with the formalism described in Sec. II one has all the tools required to compute line profiles that account for the change in the short-range atomic potentials induced by the NN interaction. In the following we consider a two-center system (F^{8+}, F^{9+}) embedded in a dense fluorine plasma. We label by (n_s,l_s,m_s) the original quantum numbers of the ion F^{8+}, which are good quantum numbers in our representation only for $R\rightarrow\infty$.

Figure 5 shows the splitting due to the NN interaction of the $n_s=3$ energy level. The variation of the transition energies is presented as a function of the internuclear distance. The energy of the transition F $3p$-$1s$ (-36 a.u.) is chosen as the reference zero energy. Calculations were performed in Fig. 5(b) for a mean electron density $N_e=2\times10^{23}$ cm^{-3} and for an electron temperature $T_e=300$ eV. These curves are compared to the ones in Fig. 5(a) for which the free electron screening effects have been removed. It can be seen in Figs. 5(a) and 5(b) that at large NN distances ($R>6$ a.u.) the various sublevels no longer depend on R and correspond to the usual Stark components. Two major effects result from the shielding of the NN interaction by plasma free electrons. A reduction of the level splitting is evident at large internuclear separations. This can be interpreted in terms of a reduction of

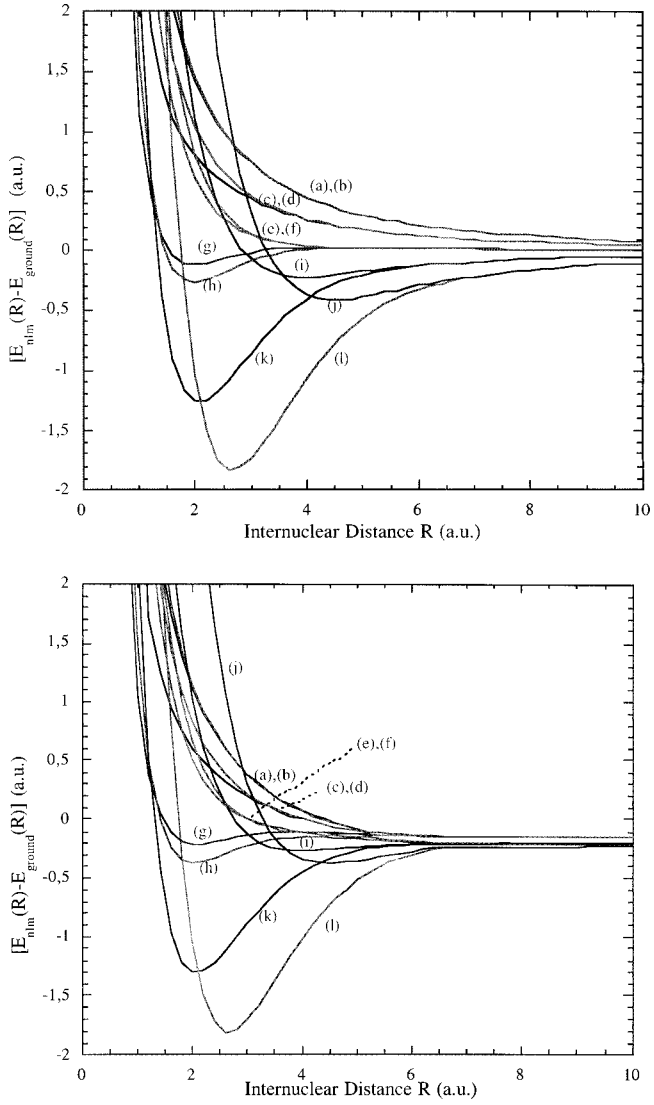

FIG. 5. Variation, as a function of the distance from its nearest neighbor, of the transition energies of a F^{+8} ion. Electron screening is considered in Fig. 6(b) (for which $N_e=2\times10^{23}$ cm^{-3} and $T_e=300$ eV) but not in Fig. 6(a) [the free-electron potential energy term V has been set to zero in Eq. (6)]. Only transition energies belonging to the spectral range of the F Ly-β line are represented. The F $3p$-$1s$ transition energy (-36 a.u.) is the reference zero energy. The transitions considered, labeled by the spherical quantum numbers nlm and the parity (gerade ''g'' or ungerade ''u'') of the upper state involved, are (a) $300g$, (b) $410u$, (c) $421g$, (d) $311u$, (e) $420g$, (f) $530u$, (g) $322g$, (h) $432u$, (i) $541g$, (j) $650u$, (k) $431u$, (l) $540g$. The ground state is formed by the states 100_g and 210_u. As a result of electron screening, we observe at large internuclear separations both a reduction of the Stark effect and a shift of all the transitions in the direction of lower energies.

the Stark effect. In addition, still for large R, all the transition energies between excited levels and the ground state are reduced by the presence of the free electrons. This is the so-called ''plasma polarization shift (PPS).'' We present in Table II the PPS of the F Lyman-β line obtained in the QM model for various plasma parameters. These results are compared to the ISM ones, computed by Nguyen *et al.* [11]. A very good agreement is found.

TABLE II. Plasma polarization shift (in a.u.) of the F Ly-β line for different plasma parameters. Our results are compared to the ones reported by Nguyen *et al.* [11] (in brackets).

T_e (eV) \ N_e (cm^{-3})	10^{23}	2×10^{23}	3×10^{23}
300	−0.11	−0.212	−0.33
	[−0.11]	[−0.217]	[−0.33]
600	−0.093	−0.18	−0.28
	[−0.092]	[−0.184]	[−0.276]

In the quasistatic theory the line profile corresponding to a transition from a group of upper levels $\alpha=\{nlm\}$ to a group of lower levels $\beta=\{n'l'm'\}$ is given by [15]

$$I(\omega)=\sum_{\alpha\beta}\int_0^\infty [dR\ P_{\rm NN}(R;N_e,T_e)f_{\alpha\beta}(R;N_e,T_e) \times\delta(\omega-\Delta E_{\alpha\beta}(R;N_e,T_e))]. \quad (10)$$

For given plasma parameters (N_e,T_e), $P_{\rm NN}(R)$ is the NN probability density and $\Delta E_{\alpha\beta}(R)$ is the transition energy. The oscillator strength $f_{\alpha\beta}(R)$ of the transition $\alpha\rightarrow\beta$ is defined by

$$f_{\alpha\beta}(R)=[E_\alpha(R)-E_\beta(R)]|\langle\phi_{\alpha=\{nlm\}}|\vec{r}|\phi_{\beta=\{n'l'm'\}}\rangle|^2 \equiv\Delta E_{\alpha\beta}(R)d^2_{\alpha\beta}(R). \quad (11)$$

The line shape formula (10) relies on two well-defined approximations. First it is assumed that the influence of the surrounding plasma ions on the atomic orbitals is well represented by the only nearest neighbor interaction. We will probe the validity of this assumption later in this paper (see Sec. IV B) on the basis of molecular dynamics microfield simulations. Second, the quasistatic approximation (namely, the change in the ionic configuration is negligible during a radiative deexcitation) is assumed to hold true. This is valid because for the plasma parameters considered in this work, where the ionic and electronic temperatures are the same, the nuclear velocities are much smaller than both the bound and free electronic velocities. Using the form (7) of the electron wave functions, the dipolar matrix elements $d_{\alpha\beta}$ can be expressed as

$$d_{\alpha\beta}(R)=\left\langle\sum_{\alpha'}a_{\alpha\alpha'}(R)\phi^{(0)}_{\alpha'}\middle|\vec{r}\middle|\sum_{\beta'}a_{\beta\beta'}(R)\phi^{(0)}_{\beta'}\right\rangle. \quad (12)$$

Defining the dipolar matrix element $d^{(0)}_{\alpha'\beta'}(R)$ corresponding to the pure one-electron diatomic molecule by

$$d^{(0)}_{\alpha'\beta'}(R)=\langle\phi^{(0)}_{\alpha'}|\vec{r}|\phi^{(0)}_{\beta'}\rangle \quad (13)$$

we have

$$d_{\alpha\beta}(R)=\sum_{\alpha'\beta'}a_{\alpha\alpha'}(R)a_{\beta\beta'}(R)d^{(0)}_{\alpha'\beta'}(R). \quad (14)$$

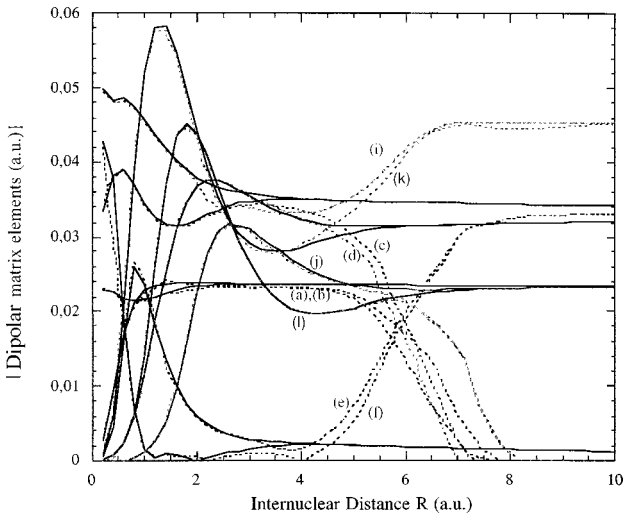

FIG. 6. Variation of the dipolar matix elements of a F^{8+} ion as a function of the distance from its nearest neighbor for $N_e=0$ (solid lines) and $N_e=2\times10^{23}$ cm^{-3}, $T_e=300$ eV (dotted lines). Notations of Fig. 5 are used to label the various dipolar matrix elements.

In elliptical coordinates the different components of the dipolar operator $\vec{r}$ are given by

$$x=\frac{R}{2}\sqrt{(\lambda^2-1)(1-\mu^2)}\cos\varphi,$$
$$y=\frac{R}{2}\sqrt{(\lambda^2-1)(1-\mu^2)}\sin\varphi, \quad (15)$$
$$z=\frac{R}{2}\lambda\mu.$$

These expressions lead to the selection rules $\Delta m=0$ for the so-called ''parallel transitions'' (i.e., z transitions) and $\Delta m=\pm1$ for the so-called ''perpendicular transitions'' (i.e., x and y transitions) [16].

Figure 6 shows the variation of the unperturbed $d^{(0)}_{\alpha'\beta'}(R)$ (solid lines) and perturbed by plasma (dotted lines) $d_{\alpha\beta}(R)$ dipolar matrix elements of the transitions considered in Fig. 5 as a function of the NN distance. The plasma conditions considered here are again $N_e=2\times10^{23}$ cm^{-3} and $T_e=300$ eV. Significant differences between $d^{(0)}_{\alpha'\beta'}(R)$ and $d_{\alpha\beta}(R)$ appear only at large internuclear separations.

To compute realistic line shapes we considered the electron collisional broadening of the various sublevels $E_\alpha(R)$. In the well-known impact approximation [15] and disregarding strong collision corrections, the electron broadening operator G is given (in atomic units) by [15,17]

$$\Gamma=\frac{4\pi}{3}N_e\left(\frac{2}{\pi T_e}\right)^{1/2}(\vec{r}\cdot\vec{r})\ln\left[\frac{Z}{n_s^2}\left(\frac{T_e}{4\pi N_e}\right)^{1/2}\right], \quad (16)$$

where the operator $\vec{r}\cdot\vec{r}$ represents the dipole-dipole interaction. We express each of the molecular states previously labeled by the spherical quantum numbers (nlm) in terms of the parabolic quantum numbers (n_1n_2m). In this last representation and neglecting the off-diagonal terms, the matrix elements of $\vec{r}\cdot\vec{r}$ can be written as

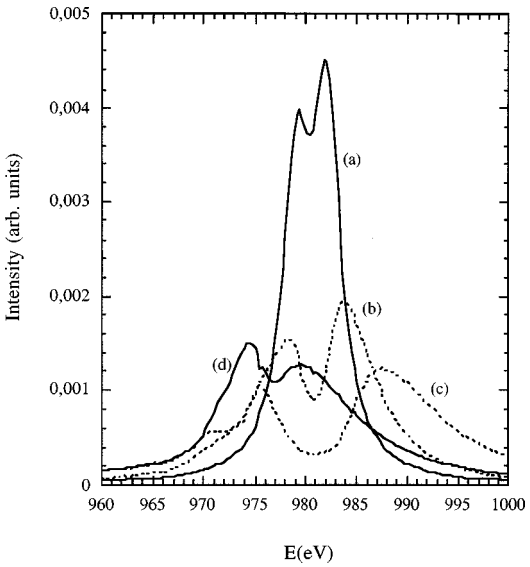

FIG. 7. F Ly-β line profiles for different electron densities N_e and for a single electron temperature. $T_e=300$ eV. Profiles (a) and (b) result from calculations with $N_e=5\times10^{22}$ cm^{-3} and profiles (c) and (d) come from computations performed for $N_e=2\times10^{23}$ cm^{-3}. For profiles (b) and (c) electron screening effects have not been included in the molecular physics calculation [the potential energy term V has been set to zero in Eq. (6)] but have been considered in the corresponding molecular dynamics simulations.

$$\langle n_1 n_2 m|\vec{r}\cdot\vec{r}|n_1 n_2 m\rangle=\sum_l\ [|\langle n_1 n_2 m|n_s l_s m\rangle|^2 \times\langle n_s l_s m|\vec{r}\cdot\vec{r}|n_s l_s m\rangle], \quad (17)$$

where (n_s,l_s,m) are the purely atomic quantum numbers. The Clebsch-Gordan coefficients $\langle n_1 n_2 m|n_s l_s m\rangle$ are expressed in terms of $3j$ symbols as [18]

$$\langle n_1 n_2 m|n_s l_s m\rangle=(-1)^{\frac{(2n_2+|m|-m)}{2}} \times(-1)^{n-1}\begin{pmatrix} \frac{n_s-1}{2} & \frac{n_s-1}{2} & l_s \\ \frac{m+q}{2} & \frac{m-q}{2} & m \end{pmatrix}, \quad (18)$$

$$q=n_2-n_1.$$

In second-order perturbation theories [19,20], the matrix elements of the dipole-dipole interaction operator in the (n_s,l_s,m) representation are

$$\langle n_s l_s m|\vec{r}\cdot\vec{r}|n_s l_s m\rangle=\frac{9n_s^2}{4Z^2}\,(n_s^2-l_s^2-l_s-1). \quad (19)$$

B. Results and discussion

We present in Fig. 7 line profiles of F Lyman-β (Ly-β) at $T_e=300$ eV for two electron density conditions, $N_e=5\times10^{22}$ cm^{-3} [curves (a) and (b)] and $N_e=2\times10^{23}$ cm^{-3} [curves (c) and (d)]. Curves (a) and (d) include the effect of the shielding of the NN interaction by free electrons whereas this influence has not been included in curves (b) and (c) [i.e., the potential energy term V has been removed from Eq. (6)]. Comparing profiles (a) and (d) in Fig. 7, it is seen that an increasing of the plasma density leads to changes both in the line shape and in the position of its center of gravity. The evolution of the line profile at large plasma densities results in fact from two separate effects, which have opposite contributions. On one hand, as the density becomes larger, the mean NN distance decreases and thus the splitting of the various sublevels is more important. This contributes to an increase in the full width at half maximum (FWHM) of the line and shifts the two main components of this line away from the central dip (in the usual terminology, this is the Stark effect). On the other hand, as the density increases, plasma screening effects are enhanced. As previously emphasized (see Sec. IV A), this leads to a reduction of the Stark effect and to a global (plasma polarization) shift of the line in the direction of lower energies. These last two effects can be seen in the figure by comparing the profiles (a) and (d) with the profiles (b) and (c), respectively. It is also important to note that the main shifting mechanism for the low-energy component of the F Ly-β line (i.e., the ''red'' component) is the Stark effect whereas the high-energy component of the line (i.e., the ''blue'' component) is strongly influenced by PPS as well.

The main assumption of our model consists in the modeling of the ion-ion interactions in terms of the only NN interaction. It is important to assess the error in the FWHM of the various profiles presented in Fig. 7 resulting from this simplified treatment. To do this, we performed MD simulations. We computed the microfield distribution produced on a central ion of interest by its NN and compared this distribution to the one obtained in the case where all the plasma ionic perturbers are considered. Results are shown in Fig. 8. The width of the Ly-β line is determined by the width of the microfield distribution. We denote the difference in FWHM of the microfield distribution between that calculated only including the NN and that resulting from all the ions as $\delta(P_{1/2})$. The simulations indicate that $\delta(P_{1/2})$ is smallest when the density is the highest [$\delta(P_{1/2})$ is 25% for $N_e=5\times10^{22}$ cm^{-3}, 18% for $N_e=2\times10^{23}$ cm^{-3}, and 14% for $N_e=10^{24}$ cm^{-3}]. This suggests that line shapes predicted by the QM model become more reliable as the density increases.

A test of the model is also provided by a direct comparison with standard line shape theories. To do this we used the code PIM PAM POUM (PPP) [21] to compute F IX Ly-β line profiles. This code is based on a two-step calculation: The Stark profile is first determined using the usual quasistatic and impact approximations for ions and electrons, respectively [15]. A frequency fluctuation model (FFM) [21,22] is then applied to include the influence of ion dynamics on line shape. We checked that this effect, not taken into account in the QM model, leads comparatively only to very minor alterations of the line shapes at the plasma parameters considered in this work. Line profile calculations are reported in Fig. 9. The PPP line shapes (solid line) are compared to the QM profiles (dotted line) for large ($N_e=2\times10^{23}$ cm^{-3}) and low ($N_e=10^{22}$ cm^{-3}) density conditions. A comparison between the two approaches is relevant as long as the only NN microfield distribution is used in the PPP simulations. Doing

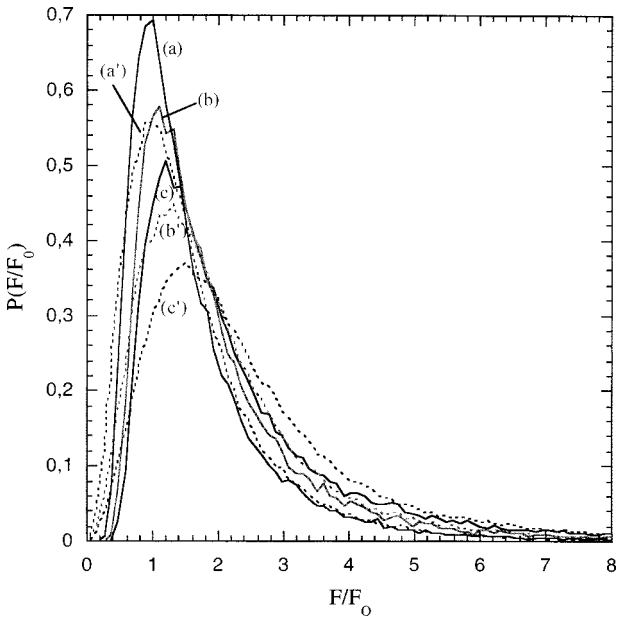

FIG. 8. Microfield distributions obtained from molecular dynamics simulations at $N_e=1\times10^{24}$ cm^{-3} [curves (a) and (a′)], $N_e=2\times10^{23}$ cm^{-3} [curves (b) and (b′)], and $N_e=5\times10^{22}$ cm^{-3} [curves (c) and (c′)]. F_0 is the mean electron field given in terms of the mean interelectronic distance r_e by $F_0=e/r_e^2$. For a given plasma condition, we compare the microfield distribution produced on a central ion of interest by its nearest neighbor (solid lines) with the one obtained in the situation where all the plasma ionic perturbers are considered (dotted lines).

this, a very good agreement is found at low density, where, in particular, the plasma free electrons have only a weak influence on the bound energy levels. We expected this result since, in our model, when the density decreases (i.e., when the average NN distance is large), the two-center bound states become pure Stark energy levels (see also the energy curves in Fig. 5 for large R). At larger density, it is seen that the high energy wing of the line is significantly shifted towards lower energies in the present approach. This results in the modification of the spectral location of the center of gravity of the line and in a reduction of its FWHM. These line shape comparisons show the important contribution of electron screening in our model.

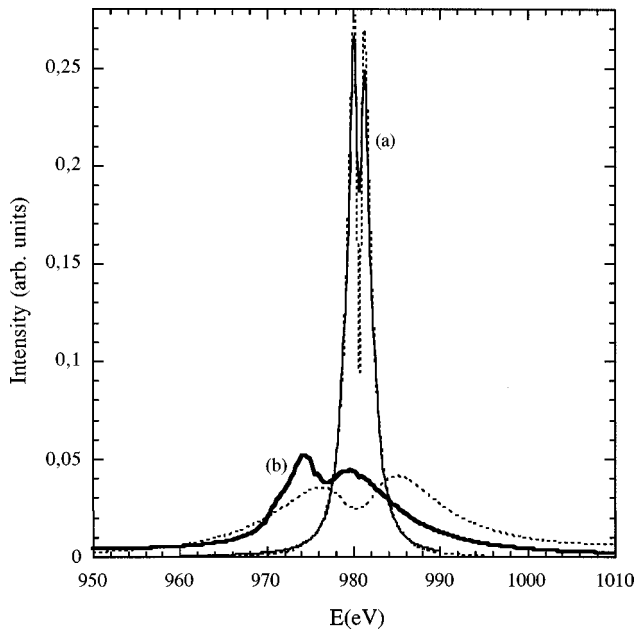

FIG. 9. F IX Ly-β line shapes at $T_e=300$ eV for $N_e=2\times10^{23}$ cm^{-3} [curves (a)] and $N_e=10^{22}$ cm^{-3} [curves (b)]. We compare the line shapes obtained in the present model (solid lines) to standard PIM, PAM, POUM simulations. In the PPP calculations the nearest neighbor microfield distribution was used. The different profiles are area normalized.

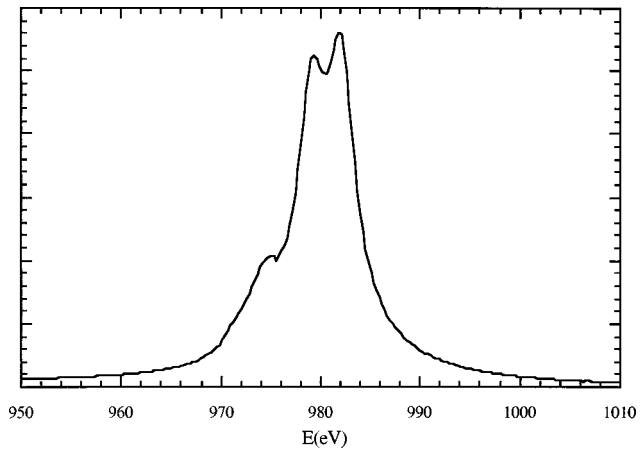

FIG. 10. F Ly-β line profile resulting from an integration over two plasma conditions: $N_e=5\times10^{22}$ cm^{-3}, $T_e=300$ eV and $N_e=2\times10^{23}$ cm^{-3}, $T_e=300$ eV. The appearance of a satellitelike feature on the low-energy wing of the line is shown and results from the shift of the line center at high density.

The interpretation of emission spectra from laser-created plasmas is usually complicated by the fact that it is rarely possible in such experiments to eliminate temporal and spatial gradients. Figure 10 gives an indication of what would be an experimental F Ly-β line shape including the effect of integration over various plasma parameters. Integration was performed over two different density conditions: $N_e=5\times10^{22}$ cm^{-3} and $N_e=2\times10^{23}$ cm^{-3}. The appearance of a satellite line on the low-energy wing of the profile is shown. This spectral feature actually results from the combined effects of integration and of the variation of the red component spectral location as a function of the density. We note that the appearance of a bump on the low-energy wing of F Ly-β observed in massive target experiments [23], and more recently in colliding foil experiments [24,25], is possibly the experimental evidence of the effect discussed here.

V. CONCLUSION

We developed in this work a two-center model aimed at describing the electronic structure of dense plasmas. This model has been used to probe the effect of ion-ion interactions on the lowering of the ionization potential. A significant reduction in the continuum-lowering depression has been shown. Our work also leads to an alternative treatment of line broadening relevant to plasma conditions where an overlapping of the excited-state orbitals from neighboring ions is expected. Calculations performed at various densities showed the sensitivity of our line shapes to electron screening.

We intend to include in a future work the contribution of electron dynamics in our line shape computations. This contribution is expected to reduce the (static) line shifts that appear in our calculations [26,27]. We also intend to more accurately quantify the influence of the second nearest neighbor. This is essential to provide a solid basis for further analysis of the electronic structure of dense plasmas in terms of multicenter wave functions.

ACKNOWLEDGMENTS

P.G. is grateful to A. Poquérusse for his comments on the microfield calculations. LULI is a CNRS Unité Mixte de Recherche No. 7605, associated with the Université Paris VI, CEA, and with the Ecole Polytechnique. Part of this work has been performed under the Human Capital and Mobility Contract No. ERBCHRXCT930377.

[1] F. J. Rogers and C. A. Iglesias, Science **263**, 50 (1994).
[2] S. J. Rose, Laser Part. Beams **9**, 869 (1991).
[3] A. Calisti, R. Stamm, and B. Talin, Phys. Rev. A **38**, 4883 (1988).
[4] R. W. Lee, J. Quant. Spectrosc. Radiat. Transf. **40**, 561 (1988).
[5] P. Malnoult *et al.*, Phys. Rev. A **40**, 1983 (1989).
[6] S. Skupsky, Phys. Rev. A **21**, 1316 (1980).
[7] M. Abramowitz, *Handbook of Mathematical Functions* (Dover Publications, New York, 1968).
[8] A. Salin, Comput. Phys. Commun. **14**, 121 (1978).
[9] J. D. Power, Philos. Trans. R. Soc. London, Ser. A **274**, 55 (1973).
[10] G. Hunter and H. O. Pritchard, J. Chem. Phys. **46**, 2148 (1967).
[11] H. Nguyen *et al.*, Phys. Rev. A **33**, 1279 (1986).
[12] B. J. Alder and T. E. Wainwright, J. Chem. Phys. **27**, 1208 (1957).
[13] B. J. Alder and T. E. Wainwright, J. Chem. Phys. **31**, 1459 (1959).
[14] E. L. Pollock and J. C. Weisheit, in *Proceedings of the International Conference on Spectral Line Shape (ICSLS)* (Walter de Gruyter and Co., Berlin, 1985), Vol. 3.
[15] H. R. Griem, *Spectral Line Broadening by Plasmas* (Academic Press, New York, 1974).
[16] R. S. Mulliken, J. Chem. Phys. **7**, 14 (1938).
[17] B. Held, C. Deutsch, and M. M. Gombert, Phys. Rev. A **29**, 896 (1984).
[18] J. W. B. Hugues, Proc. Phys. Soc. London **91**, 810 (1967).
[19] H. R. Griem, M. Blaha, and P. C. Kepple, Phys. Rev. A **19**, 2421 (1979).
[20] H. Nguyen *et al.*, Phys. Rev. A **24**, 438 (1981).
[21] R. Stamm *et al.*, Phys. Rev. A **38**, 4883 (1988).
[22] B. Talin *et al.*, Phys. Rev. A **51**, 1918 (1995).
[23] E. Leboucher-Dalimier, A. Poquérusse, and P. Angelo, Phys. Rev. E **47**, R1467 (1993).
[24] P. Gauthier *et al.*, J. Quant. Spectrosc. Radiat. Transf. **58**, 597 (1997).
[25] E. Leboucher-Dalimier *et al.*, J. Quant. Spectrosc. Radiat. Transf. **58**, 721 (1997).
[26] C. A. Iglesias, J. Quant. Spectrosc. Radiat. Transf. **54**, 181 (1995).
[27] D. B. Boercker and C. A. Iglesias, Phys. Rev. A **30**, 2771 (1984).